The thalamic reticular nucleus-lateral habenula circuit regulates depressive-like behaviors in chronic stress and chronic pain

Xiang Xu[1,4], Rui Chen[1,4], Xin-Yue Wang[1,4], Wen-Bin Jia[1], Peng-Fei Xu[1], Xiao-Qing Liu[2], Ying Zhang[3*], Xin-Feng Liu[1*], and Yan Zhang[1*]

[1]Department of Neurology, The First Affiliated Hospital of USTC, Division of Life Sciences and Medicine, University of Science and Technology of China, 230001 Hefei, China

[2]School of Basic Medical Sciences, Division of Life Sciences and Medicine, University of Science and Technology of China, 230027, Hefei, China

[3]Neuroscience Research Institute, Department of Neurobiology, School of Basic Medical Sciences, Key Laboratory for Neuroscience, Ministry of Education/National Health Commission of China, Peking University, 100191, Beijing, China

[4]These authors contributed equally

[*]Correspondence to:

Yan Zhang, E-mail: yzhang19@ustc.edu.cn (Lead contact)

Xin-Feng Liu, E-mail: xfliu2@ustc.edu.cn (X. F. L.)

Ying Zhang, E-mail: zhangyingnri@bjmu.edu.cn (Y. Z.)

Abstract

Chronic stress and chronic pain are two major predisposing factors to trigger depression. Enhanced excitatory input to the lateral habenula (LHb) has been implicated in pathophysiology of depression. However, the contribution of inhibitory transmission remains elusive. Here, we dissect an inhibitory projection from sensory thalamic reticular nucleus (sTRN) to LHb, which is activated by acute aversive stimuli. Repeated activation of the LHb-projecting sTRN neurons prevents CRS-induced depression onset and hyperexcitability of LHb neurons. Moreover, acute inhibition of sTRN-LHb circuit induces depressive-like behaviors in healthy mice, while enhancing this circuit relieves depression induced by both chronic stress and chronic pain. Intriguingly, both neuropathic pain and comorbid pain in chronic stress are unaffected by this pathway. Finally, we dissected sTRN upstream brain regions associated with stress. Together, our study demonstrates an inhibitory sTRN-LHb circuit in establishing and modulating depression, thus shedding light on potential therapeutic targets for preventing or managing depression.

Introduction

Depression is a common mood disorder and a leading cause of disability around the world. Chronic stress and chronic pain are two most common contributors that can lead to psychological dysfunctions such as depression. Alternatively, depressed patients have high incidence of pain (Simon et al., 1999). The vicious cycle of depression-pain comorbidity brings great challenge for refractory depression management (Campbell et al., 2003; Kroenke et al., 2008; Li, 2015).

The LHb is an evolutionarily conserved epithalamic nucleus in vertebrates (Bianco and Wilson, 2009). As a primary negative regulator of monoaminergic brain regions, the LHb has been implicated in encoding negative outcome and aversive behaviors (Hu et al., 2020; Matsumoto and Hikosaka, 2007). Preclinical studies revealed that the glutamatergic neurons of LHb (referred to as LHb^{GLU} neurons) can be activated instantly by aversive events (Cui et al., 2022; Zheng et al., 2022). After exposure to

chronic restraint stress or chronic pain, the mice displayed hyperactivity of the LHb^{GLU} neurons and depressive-like behaviors (Yang et al., 2018; Zheng et al., 2022; Zhou et al., 2019). On the contrary, LHb lesions or LHb neuronal suppression improves depressive-like symptoms in rodents (Yang et al., 2008; Yang et al., 2018; Zheng et al., 2022). Clinically, LHb neuronal activity is increased in patients with depression (Aizawa et al., 2013), and deep brain stimulation to inactivate LHb has been used to relieve major depression (Sartorius et al., 2010). These discoveries suggest the compelling association of LHb dysfunction with depression. The potential role of LHb in the processing of pain and analgesic signals has also been reported (Dai et al., 2022; Du et al., 2021; Shelton et al., 2012).

The maladaptive neuronal dysfunction could arise from changes in intrinsic properties or synaptic changes caused by the imbalance of presynaptic GABAergic and glutamatergic transmission (Shabel et al., 2014). The LHb receives extensive excitatory inputs from the limbic forebrain regions and basal ganglia (Hu et al., 2020). Hyperactivity of the LHb^{GLU} neurons has been linked to enhanced excitatory inputs (Li et al., 2011; Li et al., 2013; Zheng et al., 2022). Manipulation of LHb-upstream excitatory afferents, such as lateral hypothalamus (LH) (Stamatakis et al., 2016; Zheng et al., 2022), substantia innominate (Cui et al., 2022), medial prefrontal cortex (mPFC) (Lin et al., 2022), lateral preoptic areas (LPO) (Barker et al., 2017) and ventral pallidum (VP) (Liu et al., 2020), can bidirectionally regulate depressive-like behaviors. However, much less attention has been paid on the role of inhibitory afferents to LHb in pathophysiology and modulation of depression.

The thalamic reticular nucleus (TRN), a cluster of GABAergic neurons (Houser et al., 1980), is a thin, shell-like structure located between the dorsal thalamus and cerebral cortex. It receives inputs from the cortex and other thalamic nuclei. Meanwhile, the TRN provides the major inhibition to thalamic neurons and functions as a “gateway filter” in information flow between the cortex and thalamus (Crick, 1984; Halassa and Acsady, 2016; Pinault, 2004). The TRN has been elucidated in arousal, cognitive function, sensorimotor processing, defensiveness and pain

modulation (Dang-Vu et al., 2010; Dong et al., 2019; Halassa et al., 2014; Liu et al., 2022; Xi et al., 2023; Yu et al., 2009), yet the functional role of TRN-LHb circuit in depression and pain has not been explored.

Here, we found that the somatostatin-expressing neurons, rather than parvalbumin (PV)-expressing neurons in sensory TRN (referred to as $sTRN^{SOM}$ and $sTRN^{PV}$ neurons, respectively), send direct inhibitory inputs to LHb^{GLU} neurons. *In vivo* fiber photometry revealed that the TRN afferents in the LHb are instantly activated by acute aversive stimuli. Notably, repetitive activation of the sTRN-LHb circuit during CRS is sufficient to prevent depression formation by altering the excitability of LHb neurons. Furthermore, artificial manipulation of this circuit bidirectionally modulates depressive-like behaviors, rather than pain-like behaviors. Finally, whole brain mapping dissects the brain regions which are involved in signaling stress information to sTRN. Thus, this study elucidates a novel inhibitory sTRN-LHb circuit in pathophysiology and modulation of depression which provides a functional substrate for early intervention before depression onset and also for depression management.

Results

Aversive stimuli activate LHb-projecting sTRN neurons

Somatostatin-expressing and pavalbumin-expresssing neurons are two major subsets of inhibitory neurons within the TRN (Li et al., 2020). To assess the TRN-LHb projection, we injected anterograde tracing virus AAV-DIO-mCherry into the caudal part (also referred to as sTRN) or rostral part (also referred to as lTRN) of TRN in *SOM-Cre* and *PV-Cre* mice (Figures 1A, Figure S1A and S1C). Intriguingly, dense $mCherry^{+}$ fibers were detected exclusively in LHb of *SOM-Cre* mice with sTRN injection (Figures 1A-1C and Figure S1A-S1D). To exclude the passenger fibers across the LHb, the $sTRN^{SOM}$-LHb projection was further supported by retrograde trans-monosynaptic labeling by injecting AAV2/2-retro-hSyn-Cre into the LHb and AAV-DIO-mCherry into the sTRN of *C57* mice (Figure 1D and 1E), showing that ~89% of retrogradely labeled $mCherry^{+}$ neurons in sTRN overlapped with somatostain. Furthermore, AAV-based anterograde trans-monosynaptic labeling in *C57* mice

proved that sTRN-targeted LHb neurons are major (~97%) glutamatergic neurons (Figure 1F and 1G). From data, we proved that $sTRN^{SOM}$ neurons send direct projections to LHb^{GLU} neurons.

To examine functional projections from the sTRN to the LHb, AAV-DIO-ChR2-mCherry was injected into the sTRN of *SOM-Cre* mice (Figure 1H, left). The functional viral expression was proved by the reliable action potentials of ChR2-expressing $sTRN^{SOM}$ neurons following 20 Hz blue light stimulation (Figure 1H, right). Whole-cell patch-clamp recordings from the LHb neurons showed that photostimulation of $ChR2^{+}$ fibers originating in the sTRN evoked inhibitory postsynaptic currents (IPSCs), which can be blocked by bath application of bicuculline (Bic, 10 μM), a selective $GABA_A$ receptor antagonist (BIC; Figure 1I). Moreover, light-evoked IPSC was blocked by tetrodotoxin (TTX) and partially restored by potassium channel blocker 4-aminopyridine (4-AP) (Figure 1J), suggesting that LHb receives direct inhibitory inputs from the $sTRN^{SOM}$ neurons.

The LHb is perceived as a key hub for aversive information processing. In consistent with previous studies (Cui et al., 2022; Zheng et al., 2022), LHb neurons were activated in mice subjected to RS (6 h), compared with mice with fasting for solids and liquids (6 h) but remained unrestraint (Figure S2A and S2B). *In vivo* fiber photometry further demonstrated that population activity of LHb^{GLU} neurons was significantly increased upon various aversive stimuli including acute RS, air puff and tail pinch (Figure S2C-S2N). We next want to know whether the sTRN-LHb projection also processes aversive information. We recorded Ca^{2+} transients of sTRN afferents within LHb (Figure 1K). To this end, we expressed Ca^{2+} indicator GCaMP6m in sTRN and implanted an optical fiber above the LHb of *C57* mice (Figure 1L). We observed bulk calcium signals of LHb-projecting sTRN afferents in response to acute RS, air puff or tail pinch (Figure 1M-1U), suggesting that sTRN-LHb projection is also behaviorally engaged in processing aversive information.

Repeated activation of the LHb-projecting sTRN neurons prevents chronic

restraint stress (CRS)-induced depression onset by altering the excitability of LHb neurons

The balance between GABAergic and glutamatergic transmission controls LHb activity and behavior (Shabel et al., 2014). Enhanced excitatory transmission to LHb has been reported in different animal models of depression (Li et al., 2011; Li et al., 2013; Zheng et al., 2022). However, the role of inhibitory transmission of sTRN-LHb circuit in depression onset is unknown.

We resolve the question in a depression model induced by chronic stress, one of the most common factors clinically. As reported previously (Yang et al., 2018; Zhu et al., 2021), chronic restraint stress (CRS, 3 weeks restraint for 6 hours per day) induced depressive-like behaviors, including increased immobile duration in both forced swimming test (FST) and tail suspension test (TST), and decreased sucrose preference ratio in sucrose preference test (SPT) (Figure S3A and 3B). The locomotion tested in the open-field test (OFT) was not affected (Figure S3C).

Next, we assessed whether artificially enhancing LHb-projecting sTRN neural activity during CRS could prevent depression onset. We injected AAV2/2-retro-hSyn-Cre into the LHb and AAV-DIO-hM3D(Gq)-mCherry or AAV-DIO-mCherry into the sTRN of *C57* mice to activate the LHb upstream sTRN neurons during CRS (Figure 2A and 2B). The efficacy of virus expression was confirmed by depolarization of the resting membrane potentials (RMP) and neural firing by CNO in hM3Dq-expressing sTRN neurons (Figure 2C). We then intraperitoneally injected CNO prior to daily RS (6 h) for 21 days. Interestingly, we found that chronic excitation of the LHb-projecting sTRN neurons during CRS successfully prevented the development of depression in hM3Dq group, while the mCherry control mice exhibited depressive-like behaviors assessed by the FST, TST and SPT (Figure 2D-2F). The locomotion assessed by OFT was not affected by repeated activation of the LHb-projecting sTRN neurons (Figure 2G).

Given that hyperactivity of LHb neurons is closely associated with pathophysiology of depression (Lawson et al., 2017; Li et al., 2011; Li et al., 2013; Zheng et al., 2022),

we further explored whether chemogenetic excitation of the LHb-projecting sTRN neurons would prevent the hyperactivity of LHb neurons induced by CRS. First of all, we found that firing rate of LHb neurons were significantly increased in slices obtained from CRS mice compared with naïve controls (Figure S3D and S3E). Meanwhile, the LHb neurons displayed depolarized resting membrane potential (RMP) and increased input resistance in slices obtained from CRS mice compared with naïve controls (Figure S3F and S3G). However, chronic activation of the LHb-projecting sTRN neurons during CRS restored the hyperexcitablity of LHb neurons, as indicated by the decreased neural firing frequency, hyperpolarized RMP and decreased input resistance of LHb neurons in CRS-treated hM3Dq mice compared with CRS-treated mCherry controls (Figure 2H-2K). Taken together, attenuated sTRN inputs are indispensible for CRS-induced hyperactivity of LHb neurons and depression onset.

Acute inhibition of the sTRN^{SOM}-LHb circuit induces depressive-like behaviors in naïve mice

The prevention of depression onset by sTRN^{SOM}-LHb circuit activation during CRS prompted us to further examine whether acute inhibition of sTRN^{SOM}-LHb circuit would induce depressive-like behaviors in naïve mice. To this end, we injected AAV-DIO-eNpHR3.0-EYFP or AAV-DIO-EYFP into the sTRN and implanted optical fiber above the LHb of *SOM-Cre* mice (Figure 3A-3C). Current clamp recordings on eNpHR3.0-expressing sTRN^{SOM} neurons showed that 20 Hz yellow light stimulation suppressed action potentials (Figure 3D), suggesting the functional viral transduction. Behaviorally, optogenetic inhibition of the sTRN^{SOM} afferents within LHb was sufficient to induce depressive-like behaviors assessed by the TST and SPT (Figure 3E and 3F), which is similar with depressive-like behaviors induction following chemogenetic activation of LHb^{GLU} neurons (Figure S3J-S3L). The locomotion tested in OFT was unaffected by the sTRN^{SOM}-LHb inhibition or LHb^{GLU} neural activation (Figure 3G and Figure S3M). These data indicate that tonic activity of sTRN^{SOM} afferents within LHb is necessary for preventing depressive-like behaviors in naïve mice.

To further demonstrate the role of sTRN-LHb circuit in depression, we also investigated the sufficiency of sTRN-postsynaptic LHb neural activation in driving depressive-like behaviors. We injected the AAV2/1-hSyn-Cre into the bilateral sTRN and AAV-DIO-hM3D(Gq)-mCherry or AAV-DIO-mCherry into the LHb of *C57* mice (Figure 3H-3J). After 21 days viral expression, the sTRN-targeted LHb neurons expressed functional hM3Dq indicated by neural depolarization by CNO (10 μM) application (Figure 3K). The mice were then subjected to a series of depressive-like behavioral tests following i.p CNO or vehicle. We found that activation of sTRN-postsynaptic LHb neurons was also sufficient to drive depressive-like behaviors tested in FST, TST and SPT (Figure 3L-3N), without any influence on locomotion (Figure 3O). In summary, $sTRN^{SOM}$-LHb circuit inhibition induces depressive-like behaviors.

Activation of the $sTRN^{SOM}$-LHb circuit alleviates depressive-like behaviors induced by chronic stress and by chronic pain

Given that LHb neural hyperactivity underlies depression and $sTRN^{SOM}$-LHb projections are GABAergic, we postulated that activation of $sTRN^{SOM}$-LHb circuit would alleviates depression. Because chronic stress and chronic pain are two most common contributors causing depression, we thus tested the postulation on both CRS-induced depression and neuropathic pain-induced comorbid depression models.

First of all, CRS-induced depression model was studied. We injected *SOM-Cre* mice with AAV-DIO-ChR2-mCherry or AAV-DIO-mCherry into the LHb, and subsequently performed CRS for 21 days (Figure 4A-4C). After that, optical fibers were implanted above the LHb and mice were allowed for additional one-week recovery before subjecting to depression-related behavioral tests. As expected, optogenetic activation of $sTRN^{SOM}$ neural terminals within the LHb significantly rescued depressive-like behaviors tested in the TST and SPT in ChR2 group compared with mCherry controls (Figure 4D and 4E), which is in accordance with depressive-like behaviors relief induced by chemogenetic inhibition of LHb^{GLU} neurons (Figure S4A-4E). The locomotion tested in OFT was unaffected by the circuit

220 inhibition or LHb^{GLU} neural activation (Figure 4F and Figure S4F).

221 To further investigate the role of sTRN-LHb circuit in depression relief, we
222 examined whether sTRN-postsynaptic LHb neural inhibition could relieve
223 CRS-induced depressive-like behaviors. We bilaterally injected the AAV2/1-hSyn-Cre
224 into sTRN and AAV-DIO-hM4D(Gi)-mCherry or AAV-DIO-mCherry into LHb of
225 *C57* mice, which were then restrained for 21 days (Figure S4G-S4I). Patch-clamp
226 recording from hM4Di-expressing neurons in the LHb showed the hyperpolarization
227 of the resting membrane potential by CNO (Figure S4J), confirming the functionality
228 of the virus. After i.p CNO, CRS-induced depressive-like behaviors were largely
229 alleviated in hM4Di group compared with saline-treated and mCherry-injected naïve
230 controls (Figure S4K-S4M). The motor activity assessed by OFT was not affected by
231 sTRN-targeted LHb neural inhibition (Figure S4N).

232 Second, we investigated the role of sTRN-LHb circuit in comorbid depression
233 induced by chronic pain, which is one of the most common forms of drug-resistant
234 depression. Here, we used spared nerve injury (SNI) as chronic pain model (Figure
235 4G). Six weeks after operation, mice developed depressive-like symptoms in the FST,
236 TST and SPT assays (Figure S5A and S5B), without any deficit on locomotion
237 activity (Figure S5C). Chemogenetic inhibition of LHb^{GLU} neurons can greatly relieve
238 neuropathic pain-induced comorbid depressive-like behaviors (Figure S5D-S5G)
239 without any influence on locomotion (Figure S5H), suggesting the involvement of
240 LHb in comorbid depression under chronic pain as previously reported (Zhou et al.,
241 2019). Moreover, either optogenetic activation of $sTRN^{SOM}$ neural afferents within the
242 LHb (Figure 4G-4K) or the specific inhibition of sTRN-targeted LHb neurons (Figure
243 S5I-S5L) can efficiently alleviate comorbid depression in neuropathic pain, as
244 observed in CRS model. The locomotion was unaltered by both manipulations (Figure
245 4L and Figure S5M). Taken together, enhancing $sTRN^{SOM}$-LHb circuit can rescue
246 depressive-like behaviors induced by both chronic stress and chronic pain.

247 **Activation of the $sTRN^{SOM}$-LHb circuit does not affect pain induced by nerve**
248 **injury and by depression**

249 Besides the pivotal role in depression, the LHb was also involved in pain processing
250 (Dai et al., 2022; Du et al., 2021; Shelton et al., 2012). We next investigated whether
251 sTRN^{SOM}-LHb circuit activation would affect pain in two pain models: SNI-induced
252 neuropathic pain and comorbid pain in depression. Surprisingly, sTRN^{SOM}-LHb
253 circuit activation did not relieve the SNI-induced mechanical hypersensitivity (Figure
254 5A-5C). Given high incidence of comorbid pain in depressive patients, we repeated
255 the experiment as performed in SNI model. As previous study (Zhu et al., 2021), the
256 mice displayed marked mechanical hypersensitivity until three weeks-CRS when
257 depressive-like behaviors developed, and the comorbid pain last at least two weeks
258 after termination of CRS (Figure 5D and 5E). Next, we evaluated the effect of
259 sTRN^{SOM}-LHb circuit activation on pain threshold within the two weeks-time window.
260 We observed that mechanical hypersensitivity induced by CRS was also unaffected
261 (Figure 5F). Collectively, our data indicate that sTRN^{SOM}-LHb circuit specifically
262 modulates depression rather than pain.

263 **sTRN upstream brain regions activated by restraint stress**

264 As early as 1984, the TRN was described as "guardian of the gateway" in the
265 thalamocortical circuit (Crick, 1984). We finally investigate its upstream brain regions
266 that are potentially associated with stress encoding. To do this,
267 AAV2/2-retro-hSyn-Cre was injected into sTRN of *Ai14* mice (Figure S6A). Three
268 weeks later when sTRN upstream brain areas were labeled, mice were further exposed
269 to RS (6h) or remained undisturbed (Figure S6A). We found that sTRN received
270 broad presynaptic inputs from various brain regions (Figure S6B), including central
271 amygdala (CeA), basolateral amygdala (BLA), ventral medial nucleus (VM), anterior
272 cingulate cortex (ACC), insular cortex (IC) and dorsal raphe nucleus (DRN). Within
273 these brain areas, we observed many c-Fos-positive neurons in mice exposed to 6h RS
274 while rare signals were detected in undisturbed controls (Figure S6C and S6E-6I).
275 Moreover, a small percentage of tdTomato-positive neurons in these areas were
276 co-labeled with c-Fos (Figure S6D and S6E-S6I). Together, our data suggest that
277 sTRN receives inputs from wide brain regions that are associated with stress

information processing.

Discussion

In this study, we report a previously unknown function of the TRN in thalamic control of depression. We reported three major findings. First, the LHb^{GLU} neurons receive inhibitory input from sensory TRN which can be activated by acute aversive stimuli. Second, repeated activation of the LHb-projecting sTRN neurons prevents CRS-induced depression onset by altering hyperexcitability of LHb neurons. Last, the $sTRN^{SOM}$-LHb pathway specifically restores depressive-like behaviors induced by chronic stress and chronic pain, rather than pain-like behaviors induced by nerve injury and depression.

sTRN-LHb monosynaptic inhibitory projections

Thalamic inhibition is a critical element of thalamic projecting neurons modulation, and its perturbation is found in many diseases (Halassa and Acsady, 2016). The TRN is one of the major sources of thalamic inhibition (Pinault, 2004). The neurons within TRN are highly heterogeneous in anatomical distribution, molecular identities, electrophysiological properties, synaptic connectivity and function (Brunton and Charpak, 1997; Clemente-Perez et al., 2017; Cox et al., 1996; Li et al., 2020; Martinez-Garcia et al., 2020). Although previous studies have reported hierarchical connectivity between TRN and distinct thalamic areas, for example, the core region of TRN projects to first-order thalamic nuclei whereas the shell region of TRN projects to the high-order thalamic nuclei (Li et al., 2020), and dorsal TRN predominantly projected to the posterior thalamic nucleus (Po) whereas the ventral TRN mainly innervated the ventrobasal thalamus (VB) (Liu et al., 2022), the anatomical connectivity and function of TRN-LHb projections are not yet reported.

We performed cell-specific anterograde tracing experiments, and observed that PV^+ and SOM^+ neurons in the sTRN have different projection areas. SOM^+ neurons of caudal sector of TRN (referred to as sTRN) broadly projected to LHb, ventrolateral part of the laterodorsal thalamus (LDVL), mediorostral part of the lateral posterior

thalamus (LPMR), VB, Po and ventrolateral thalamus (VL). Further retrograde monosynaptic tracing and electrophysiological results confirmed the inhibitory projections of sTRN^{SOM}-LHb. In contrast, PV^{+} neurons of the sTRN predominantly projected to VB, Po and VL, with sparse projection to LDVL and LPMR, and without projection to LHb. This complementary innervation of the dorsal thalamus by molecularly diverse neurons within sTRN enriches the understanding of a comprehensive architecture of the TRN-thalamic nuclei connectivity, and could be the neural substrates for segregated emotion (i.e., depression) and somatosensation (i.e., pain) modulation. The suspect is supported by our data showing that TRN^{SOM}-LHb projections modulate depression rather than pain, and by previous studies showing that the TRN-VB projections contribute to pain regulation (Liu et al., 2022; Zhang et al., 2017). It remains to be determined whether the TRN-VB circuit also regulates depression.

sTRN^{SOM}-LHb projections in depression onset under chronic stress

Despite much evidence on the involvement of LHb aberrant hyperactivity in depressive disorder (Aizawa et al., 2013; Yang et al., 2018; Zheng et al., 2022; Zhou et al., 2019), the neural circuit mechanisms underlying abnormal LHb activity and depression under stress have remained elusive, especially from the inhibitory circuit perspective. By using *in vivo* calcium imaging, we demonstrated that LHb-projecting inhibitory sTRN afferents are activated by aversive stimuli including acute physical restraint, suggesting their involvement in the aversive emotion encoding which has not been reported previously. To further examine the TRN-LHb inhibitory projections in pathophysiology of depression, we repetitively activate LHb-upstream sTRN neurons during CRS, and intriguingly found that both CRS-induced LHb neural hyperactivity and depression onset were prevented. Moreover, artificially silencing the sTRN^{SOM}-LHb circuit is sufficient to induce depressive-like behaviors in naïve mice. These data collectively suggest that the TRN-LHb inhibitory projection is likely involved in pathophysiology of depression during CRS. In combination with previously well elucidated enhanced excitatory inputs to LHb during chronic stress

335 (Li et al., 2011; Li et al., 2013; Zheng et al., 2022), our findings advance better
336 understanding of excitation/inhibition imbalance in hyperactive LHb neural activity
337 and pathophysiology of depression.

338 **sTRN^{SOM}-LHb projections restore depression in chronic stress and chronic pain**

339 Here, we tested two independent depressive-like mouse models: the chronic restraint
340 stress-induced depression and chronic pain-induced comorbid depression. Either
341 specific activation of LHb-projecting sTRN^{SOM} afferents or inhibition of
342 sTRN-targeted postsynaptic LHb neurons is sufficient to rescue the depressive-like
343 behaviors in above two models. Given the involvement of LHb in processing pain
344 information and analgesic signals (Dai et al., 2022; Du et al., 2021; Shelton et al.,
345 2012), we also assessed the role of sTRN-LHb pathway in pain regulation.
346 Unexpectedly, the same manipulation of sTRN-LHb circuit does not affect pain in
347 both nerve injury-induced pain model and CRS-induced comorbid pain model. The
348 segregation control of depression and pain might arise from the possibility that
349 depression-specific ensembles in the LHb, rather than pain-specific neurons, are
350 targeted by sTRN. Future activity-dependent cellular labeling system should be
351 warranted to dissect the different subpopulation of LHb neurons processing pain and
352 depression, and their respective connections with TRN.

353 In addition, previous studies reported that PV^{+} and SOM^{+} neurons in TRN receive
354 projections from brain areas that mainly related to sensory and emotional processing,
355 respectively (Clemente-Perez et al., 2017; Martinez-Garcia et al., 2020). The
356 divergent control of different events could arise from distinct synaptic inputs and
357 intrinsic physiological characteristics of TRN cell types, shaping distinct spiking
358 outputs and thus tuning to discrete behavioral events (Clemente-Perez et al., 2017;
359 Martinez-Garcia et al., 2020). We dissected upstream brain regions of sTRN which
360 were activated by stress, including CeA/BLA, ACC, IC and DRN. These areas were
361 all implicated in emotion encoding (Beyeler et al., 2018; Cui et al., 2017; Lamm and
362 Singer, 2010; Paquelet et al., 2022; Rolls, 2019; Steinberg et al., 2020). How cell-type
363 based circuit-specific temporal tuning is involved in depression and pain processing is

interesting.

Overall, our study dissected a novel GABAergic sTRN-LHb pathway which bridges the gap in the inhibitory circuit mechanisms underlying pathophysiology of depression. We demonstrated that repetitive sTRN-LHb circuit activation during chronic stress can prevent depression onset, and transient sTRN-LHb circuit activation can alleviate depression in chronic stress or chronic pain, shedding light on early intervention targets before depression onset and therapeutic targets for depression management.

References

Aizawa, H., Cui, W., Tanaka, K., and Okamoto, H. (2013). Hyperactivation of the habenula as a link between depression and sleep disturbance. Frontiers in human neuroscience *7*, 826.

Barker, D.J., Miranda-Barrientos, J., Zhang, S., Root, D.H., Wang, H.L., Liu, B., Calipari, E.S., and Morales, M. (2017). Lateral Preoptic Control of the Lateral Habenula through Convergent Glutamate and GABA Transmission. Cell reports *21*, 1757-1769.

Beyeler, A., Chang, C.J., Silvestre, M., Leveque, C., Namburi, P., Wildes, C.P., and Tye, K.M. (2018). Organization of Valence-Encoding and Projection-Defined Neurons in the Basolateral Amygdala. Cell reports *22*, 905-918.

Bianco, I.H., and Wilson, S.W. (2009). The habenular nuclei: a conserved asymmetric relay station in the vertebrate brain. Philosophical transactions of the Royal Society of London Series B, Biological sciences *364*, 1005-1020.

Bourquin, A.F., Suveges, M., Pertin, M., Gilliard, N., Sardy, S., Davison, A.C., Spahn, D.R., and Decosterd, I. (2006). Assessment and analysis of mechanical allodynia-like behavior induced by spared nerve injury (SNI) in the mouse. Pain *122*, 14 e11-14.

Brunton, J., and Charpak, S. (1997). Heterogeneity of cell firing properties and opioid sensitivity in the thalamic reticular nucleus. Neuroscience *78*, 303-307.

Campbell, L.C., Clauw, D.J., and Keefe, F.J. (2003). Persistent pain and depression: a biopsychosocial perspective. Biological psychiatry *54*, 399-409.

Chaplan, S.R., Bach, F.W., Pogrel, J.W., Chung, J.M., and Yaksh, T.L. (1994). Quantitative assessment of tactile allodynia in the rat paw. J Neurosci Methods *53*, 55-63.

Clemente-Perez, A., Makinson, S.R., Higashikubo, B., Brovarney, S., Cho, F.S., Urry, A., Holden, S.S., Wimer, M., David, C., Fenno, L.E*., et al.* (2017). Distinct Thalamic Reticular Cell Types Differentially Modulate Normal and Pathological Cortical Rhythms. Cell reports *19*, 2130-2142.

Cox, C.L., Huguenard, J.R., and Prince, D.A. (1996). Heterogeneous axonal arborizations of rat thalamic reticular neurons in the ventrobasal nucleus. The Journal of comparative neurology *366*, 416-430.

Crick, F. (1984). Function of the thalamic reticular complex: the searchlight hypothesis. Proceedings of the National Academy of Sciences of the United States of America *81*, 4586-4590.

Cui, Y., Huang, X., Huang, P., Huang, L., Feng, Z., Xiang, X., Chen, X., Li, A., Ren, C., and Li, H. (2022). Reward ameliorates depressive-like behaviors via inhibition of the substantia innominata to the lateral habenula projection. Science advances *8*, eabn0193.

Cui, Y., Lv, G., Jin, S., Peng, J., Yuan, J., He, X., Gong, H., Xu, F., Xu, T., and Li, H. (2017). A Central Amygdala-Substantia Innominata Neural Circuitry Encodes Aversive Reinforcement Signals. Cell reports *21*, 1770-1782.

Dai, D., Li, W., Chen, A., Gao, X.F., and Xiong, L. (2022). Lateral Habenula and Its Potential Roles in Pain and Related Behaviors. ACS chemical neuroscience *13*, 1108-1118.

Dang-Vu, T.T., McKinney, S.M., Buxton, O.M., Solet, J.M., and Ellenbogen, J.M. (2010). Spontaneous brain rhythms predict sleep stability in the face of noise. Current biology : CB *20*, R626-627.

Dong, P., Wang, H., Shen, X.F., Jiang, P., Zhu, X.T., Li, Y., Gao, J.H., Lin, S., Huang, Y., He, X.B*., et al.* (2019). A novel cortico-intrathalamic circuit for flight behavior. Nature neuroscience *22*, 941-949.

Du, Y., Wu, Y.X., Guo, F., Qu, F.H., Hu, T.T., Tan, B., Wang, Y., Hu, W.W., Chen, Z., and Zhang, S.H. (2021). Lateral Habenula Serves as a Potential Therapeutic Target for Neuropathic Pain.

Neuroscience bulletin *37*, 1339-1344.
Halassa, M.M., and Acsady, L. (2016). Thalamic Inhibition: Diverse Sources, Diverse Scales. Trends in neurosciences *39*, 680-693.
Halassa, M.M., Chen, Z., Wimmer, R.D., Brunetti, P.M., Zhao, S., Zikopoulos, B., Wang, F., Brown, E.N., and Wilson, M.A. (2014). State-dependent architecture of thalamic reticular subnetworks. Cell *158*, 808-821.
Houser, C.R., Vaughn, J.E., Barber, R.P., and Roberts, E. (1980). GABA neurons are the major cell type of the nucleus reticularis thalami. Brain research *200*, 341-354.
Hu, H., Cui, Y., and Yang, Y. (2020). Circuits and functions of the lateral habenula in health and in disease. Nature reviews Neuroscience *21*, 277-295.
Kroenke, K., Shen, J., Oxman, T.E., Williams, J.W., Jr., and Dietrich, A.J. (2008). Impact of pain on the outcomes of depression treatment: results from the RESPECT trial. Pain *134*, 209-215.
Lamm, C., and Singer, T. (2010). The role of anterior insular cortex in social emotions. Brain structure & function *214*, 579-591.
Lawson, R.P., Nord, C.L., Seymour, B., Thomas, D.L., Dayan, P., Pilling, S., and Roiser, J.P. (2017). Disrupted habenula function in major depression. Molecular psychiatry *22*, 202-208.
Li, B., Piriz, J., Mirrione, M., Chung, C., Proulx, C.D., Schulz, D., Henn, F., and Malinow, R. (2011). Synaptic potentiation onto habenula neurons in the learned helplessness model of depression. Nature *470*, 535-539.
Li, J.X. (2015). Pain and depression comorbidity: a preclinical perspective. Behavioural brain research *276*, 92-98.
Li, K., Zhou, T., Liao, L., Yang, Z., Wong, C., Henn, F., Malinow, R., Yates, J.R., 3rd, and Hu, H. (2013). betaCaMKII in lateral habenula mediates core symptoms of depression. Science *341*, 1016-1020.
Li, Y., Lopez-Huerta, V.G., Adiconis, X., Levandowski, K., Choi, S., Simmons, S.K., Arias-Garcia, M.A., Guo, B., Yao, A.Y., Blosser, T.R.*, et al.* (2020). Distinct subnetworks of the thalamic reticular nucleus. Nature *583*, 819-824.
Lin, S., Huang, L., Luo, Z.C., Li, X., Jin, S.Y., Du, Z.J., Wu, D.Y., Xiong, W.C., Huang, L., Luo, Z.Y.*, et al.* (2022). The ATP Level in the Medial Prefrontal Cortex Regulates Depressive-like Behavior via the Medial Prefrontal Cortex-Lateral Habenula Pathway. Biological psychiatry *92*, 179-192.
Liu, B., Cao, Y., Wang, J., and Dong, J. (2020). Excitatory transmission from ventral pallidum to lateral habenula mediates depression. The world journal of biological psychiatry : the official journal of the World Federation of Societies of Biological Psychiatry *21*, 627-633.
Liu, P.F., Wang, Y., Xu, L., Xiang, A.F., Liu, M.Z., Zhu, Y.B., Jia, X., Zhang, R., Li, J.B., Zhang, L.*, et al.* (2022). Modulation of itch and pain signals processing in ventrobasal thalamus by thalamic reticular nucleus. iScience *25*, 103625.
Martinez-Garcia, R.I., Voelcker, B., Zaltsman, J.B., Patrick, S.L., Stevens, T.R., Connors, B.W., and Cruikshank, S.J. (2020). Two dynamically distinct circuits drive inhibition in the sensory thalamus. Nature *583*, 813-818.
Matsumoto, M., and Hikosaka, O. (2007). Lateral habenula as a source of negative reward signals in dopamine neurons. Nature *447*, 1111-1115.
Paquelet, G.E., Carrion, K., Lacefield, C.O., Zhou, P., Hen, R., and Miller, B.R. (2022). Single-cell activity and network properties of dorsal raphe nucleus serotonin neurons during emotionally salient behaviors. Neuron *110*, 2664-2679 e2668.
Pinault, D. (2004). The thalamic reticular nucleus: structure, function and concept. Brain research

Brain research reviews *46*, 1-31.
Rolls, E.T. (2019). The cingulate cortex and limbic systems for emotion, action, and memory. Brain structure & function *224*, 3001-3018.
Sartorius, A., Kiening, K.L., Kirsch, P., von Gall, C.C., Haberkorn, U., Unterberg, A.W., Henn, F.A., and Meyer-Lindenberg, A. (2010). Remission of major depression under deep brain stimulation of the lateral habenula in a therapy-refractory patient. Biological psychiatry *67*, e9-e11.
Shabel, S.J., Proulx, C.D., Piriz, J., and Malinow, R. (2014). Mood regulation. GABA/glutamate co-release controls habenula output and is modified by antidepressant treatment. Science *345*, 1494-1498.
Shelton, L., Becerra, L., and Borsook, D. (2012). Unmasking the mysteries of the habenula in pain and analgesia. Progress in neurobiology *96*, 208-219.
Simon, G.E., VonKorff, M., Piccinelli, M., Fullerton, C., and Ormel, J. (1999). An international study of the relation between somatic symptoms and depression. The New England journal of medicine *341*, 1329-1335.
Stamatakis, A.M., Van Swieten, M., Basiri, M.L., Blair, G.A., Kantak, P., and Stuber, G.D. (2016). Lateral Hypothalamic Area Glutamatergic Neurons and Their Projections to the Lateral Habenula Regulate Feeding and Reward. The Journal of neuroscience : the official journal of the Society for Neuroscience *36*, 302-311.
Steinberg, E.E., Gore, F., Heifets, B.D., Taylor, M.D., Norville, Z.C., Beier, K.T., Foldy, C., Lerner, T.N., Luo, L., Deisseroth, K.*, et al.* (2020). Amygdala-Midbrain Connections Modulate Appetitive and Aversive Learning. Neuron *106*, 1026-1043 e1029.
Xi, K., Xiao, H., Huang, X., Yuan, Z., Liu, M., Mao, H., Liu, H., Ma, G., Cheng, Z., Xie, Y.*, et al.* (2023). Reversal of hyperactive higher-order thalamus attenuates defensiveness in a mouse model of PTSD. Science advances *9*, eade5987.
Yang, L.M., Hu, B., Xia, Y.H., Zhang, B.L., and Zhao, H. (2008). Lateral habenula lesions improve the behavioral response in depressed rats via increasing the serotonin level in dorsal raphe nucleus. Behavioural brain research *188*, 84-90.
Yang, Y., Cui, Y., Sang, K., Dong, Y., Ni, Z., Ma, S., and Hu, H. (2018). Ketamine blocks bursting in the lateral habenula to rapidly relieve depression. Nature *554*, 317-322.
Yu, X.J., Xu, X.X., He, S., and He, J. (2009). Change detection by thalamic reticular neurons. Nature neuroscience *12*, 1165-1170.
Zhang, C., Chen, R.X., Zhang, Y., Wang, J., Liu, F.Y., Cai, J., Liao, F.F., Xu, F.Q., Yi, M., and Wan, Y. (2017). Reduced GABAergic transmission in the ventrobasal thalamus contributes to thermal hyperalgesia in chronic inflammatory pain. Scientific reports *7*, 41439.
Zheng, Z., Guo, C., Li, M., Yang, L., Liu, P., Zhang, X., Liu, Y., Guo, X., Cao, S., Dong, Y.*, et al.* (2022). Hypothalamus-habenula potentiation encodes chronic stress experience and drives depression onset. Neuron *110*, 1400-1415 e1406.
Zhou, W., Jin, Y., Meng, Q., Zhu, X., Bai, T., Tian, Y., Mao, Y., Wang, L., Xie, W., Zhong, H.*, et al.* (2019). A neural circuit for comorbid depressive symptoms in chronic pain. Nature neuroscience *22*, 1649-1658.
Zhu, X., Tang, H.D., Dong, W.Y., Kang, F., Liu, A., Mao, Y., Xie, W., Zhang, X., Cao, P., Zhou, W.*, et al.* (2021). Distinct thalamocortical circuits underlie allodynia induced by tissue injury and by depression-like states. Nature neuroscience *24*, 542-553.

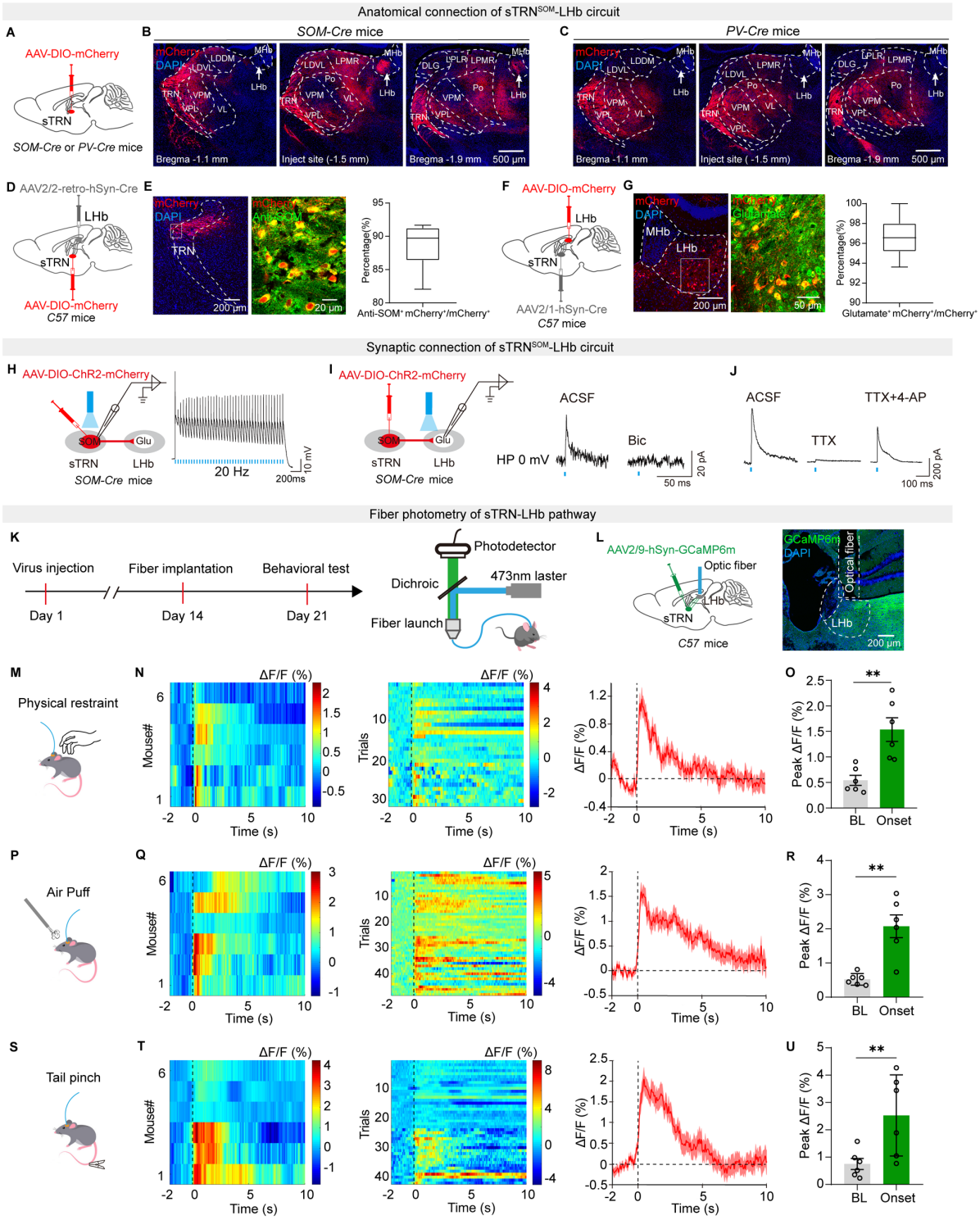

503 **Figure 1. Aversive stimuli activate LHb-projecting sTRN afferents.**

504 (A) Schematic showing viral injection into the sensory TRN of *SOM-Cre* or *PV-Cre*

505 mice.

506 (B and C) Representative images of mCherry-expressing signals in different brain

507 regions of *SOM-Cre* (B) or *PV-Cre* (C) mice. Scale bars, 500 μm.

508 (D and E) Schematic of the Cre-dependent retrograde trans-monosynaptic tracing

509 strategy in *C57* mice (D) and summary data for percentage of mCherry$^+$ neurons in
510 the sTRN which co-localize with anti-SOM immunofluorescence (E). Scale bars, 200
511 μm and 20 μm. (n=6 sections from three mice)
512 (F and G) Schematic of the Cre-dependent anterograde trans-monosynaptic tracing
513 strategy in *C57* mice (F) and summary data for percentage of mCherry$^+$ neurons in the
514 LHb which co-localize with anti-Glutamate immunofluorescence (G). Scale bars, 200
515 μm and 50 μm. (n=10 sections from five mice)
516 (H) Schematic showing sTRN electrophysiological recordings in acute slices from
517 *SOM-Cre* mice (left) and a representative trace of blue light (473 nm, 20 Hz)-evoked
518 action potentials in a ChR2-mCherry-expressing sTRN neuron (right).
519 (I) Schematic showing LHb electrophysiological recordings in acute slices from
520 *SOM-Cre* mice (left) and representative traces of light-evoked IPSCs of sTRN
521 neurons before (ACSF) and after bicuculline (Bic, 10 μM) treatment.
522 (J) Representative traces of light-evoked IPSCs of the LHb neurons before (ACSF)
523 and after TTX (1 μM) or TTX and 4-AP (500 μM) treatment.
524 (K) Schematic of experimental design (left) and fiber photometry recording *in vivo*
525 (right).
526 (L) Illustration (left) and representative image (right) of viral delivery and optic fiber
527 implantation. Scale bar, 200 μm.
528 (M, P and S) Schematic of fiber photometry recording in response to RS (M), air puff
529 (P) and tail pinch (S).
530 (N, Q and T) Heatmap and average responses showing Ca^{2+} transients evoked by RS
531 (N), air puff (Q) and tail pinch (T) in the LHb neurons. (n=6 mice/group)
532 (O, R and U) Quantification of peak average Ca^{2+} responses before and after RS (O),
533 air puff (R) and tail pinch (U) stimulation (right). (n=6 mice/group)
534 For (E) and (G), data are shown as box and whisker plots (medians, quartiles (boxes)
535 and ranges minimum to maximum (whiskers)); For (O), (R) and (U), data are
536 presented as mean ± SEM. "ns", no significance; **$p < 0.01$. Paired two-sided t test
537 for (O), (R) and (U).

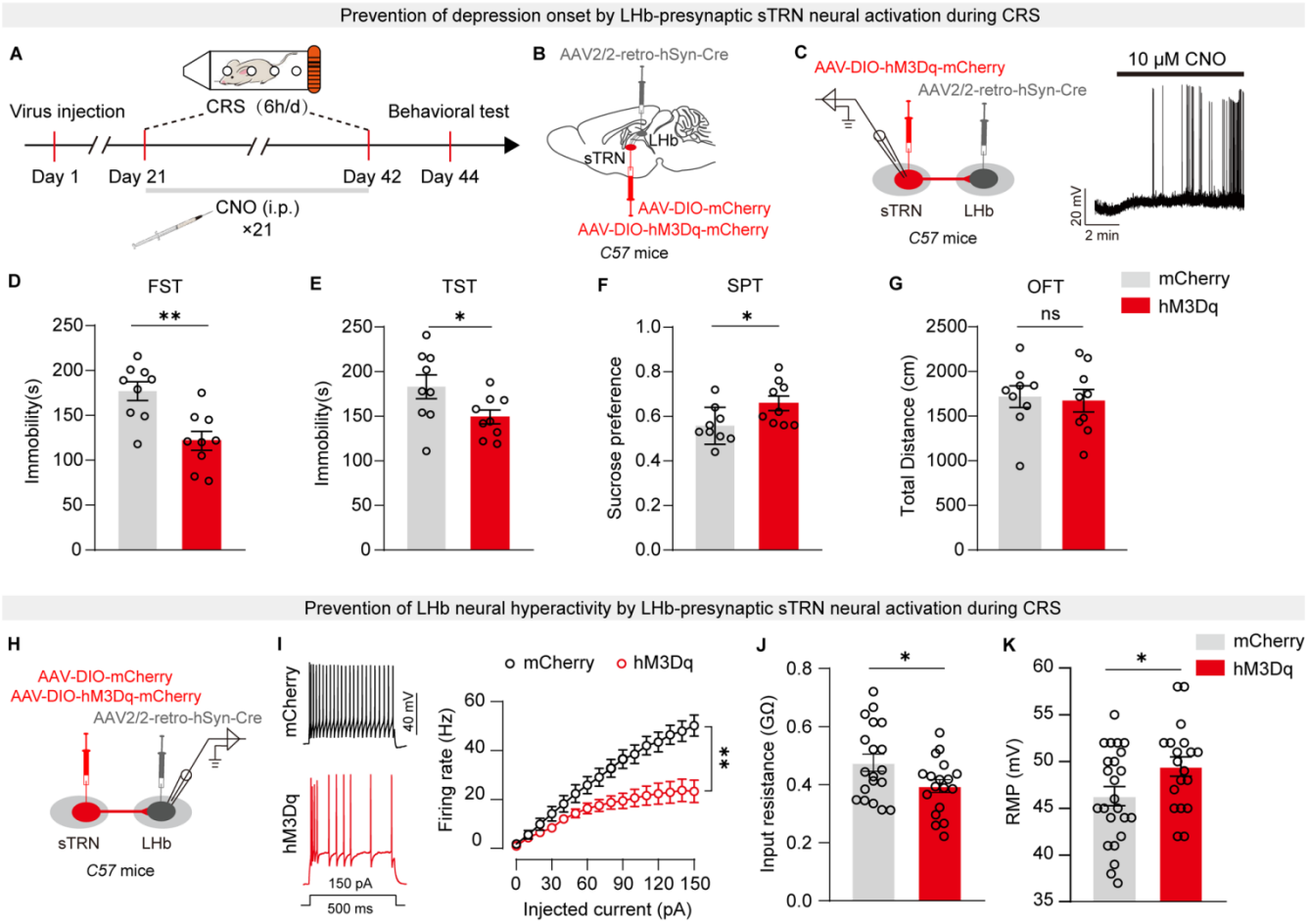

Figure 2. Repeated activation of the LHb-projecting sTRN neurons prevents CRS-induced depression onset by altering the excitability of LHb neurons.

(A) Schematic of experimental design.

(B) Illustration of viral delivery.

(C) Schematic showing sTRN electrophysiological recordings in acute slices (left) and a representative trace showing hypolarization of the hM3Dq-mCherry-expressing sTRN neuron by CNO (10 μM).

(D-G) Behavioral effects of repeated activation of the LHb-projecting sTRN neurons during CRS on depressive-like behaviors assessed by FST (D), TST (E) and SPT (F), and locomotion activity assessed by OFT (G) in *C57* mice. (n=9 mice/group)

(H) Schematic showing LHb electrophysiological recordings in acute slices.

(I-K) Summary data for the firing rate (I), input resistance (J) and resting membrane potential (K) recorded from LHb neurons of mCherry&CRS or hM3Dq&CRS mice. Data are presented as mean ± SEM. "ns", no significance; *$p < 0.05$, **$p < 0.01$.

Unpaired two-sided t test for (D-G), (J) and (K); Two-way repeated measures ANOVA with Bonferroni *post hoc* analysis for (I).

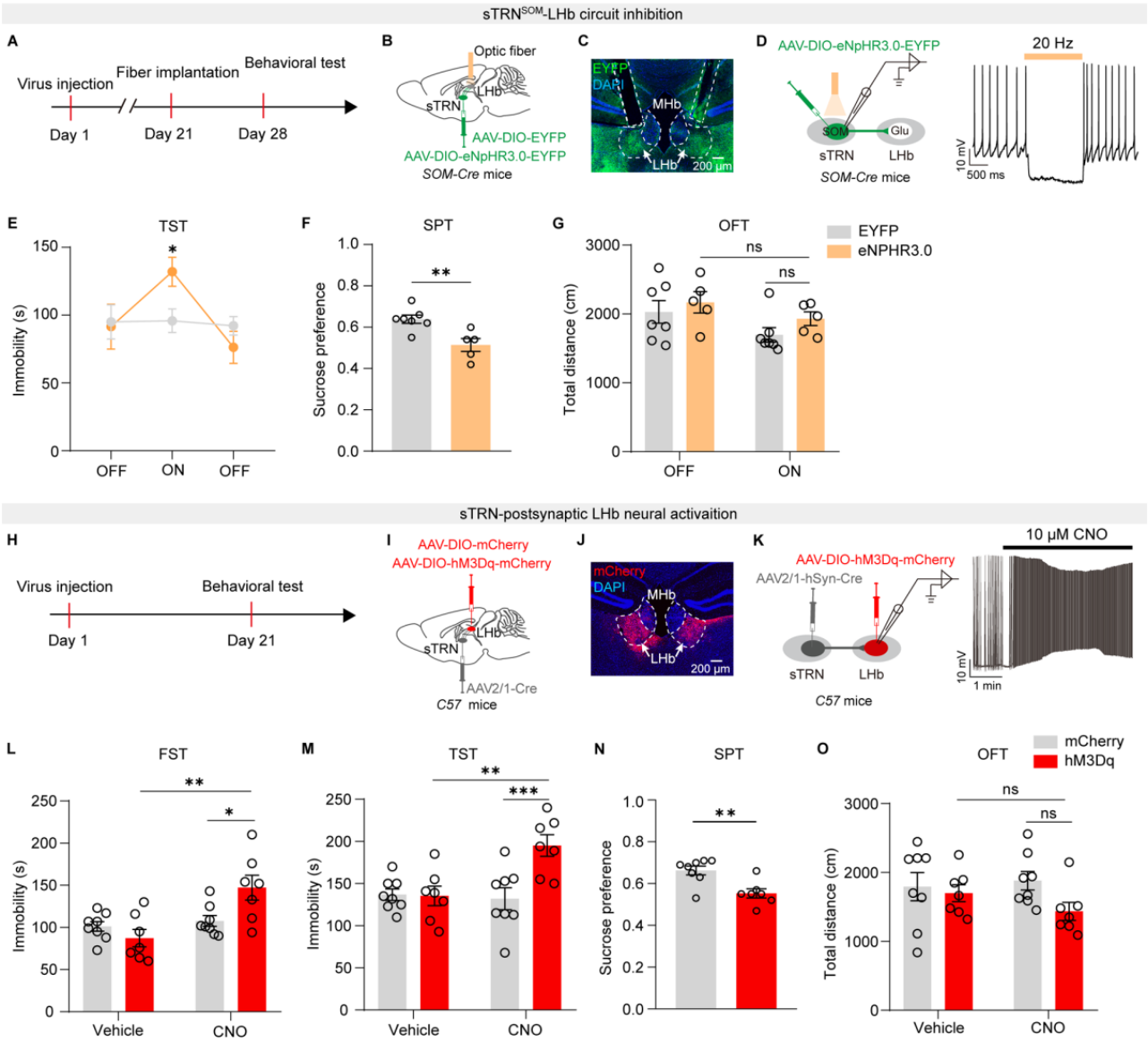

554 **Figure 3. Acute inhibition of the sTRN^{SOM}-LHb circuit induces depressive-like**
555 **behaviors in naïve mice.**
556 (A and H) Schematic of experimental design.
557 (B and C) Illustration (B) and representative image (C) of viral delivery and bilateral
558 optic fibers implantation. Scale bar, 200 μm.
559 (D) Schematic of recording configuration in acute slices and representative trace
560 showing suppression of action potentials in an eNpHR3.0-EYFP^{+} sTRN neuron by
561 laser stimulation (584 nm, 20 Hz).
562 (E-G) Behavioral effects of optogenetic inhibition of sTRN^{SOM}-LHb circuit on
563 depressive-like behaviors assessed by TST (E) and SPT (F), and locomotion activity
564 assessed by OFT (G) in naïve *SOM-Cre* mice. (n=5-7 mice/group)

565 (I and J) Illustration (I) and representative image (J) of viral delivery. Scale bar, 200
566 μm.
567 (K) Schematic of recording configuration in acute slices and representative trace
568 showing depolarization of membrane potential in a hM3Dq-mCherry^{+} LHb neuron by
569 CNO (10 μM).
570 (L-O) Behavioral effects of chemogenetic activation of sTRN-postsynaptic LHb
571 neurons on depressive-like behaviors assessed by FST (L), TST (M) and SPT (N), and
572 locomotion activity assessed by OFT (O) in naïve *C57* mice. (n=7-8 mice/group)
573 Data are presented as mean ± SEM. "ns", no significance; *$p < 0.05$, **$p < 0.01$, ***p
574 < 0.001. Two-way repeated measures ANOVA with Bonferroni *post hoc* analysis for
575 (E), (G), (L) (M) and (O); Unpaired two-sided t test for (F) and (N).

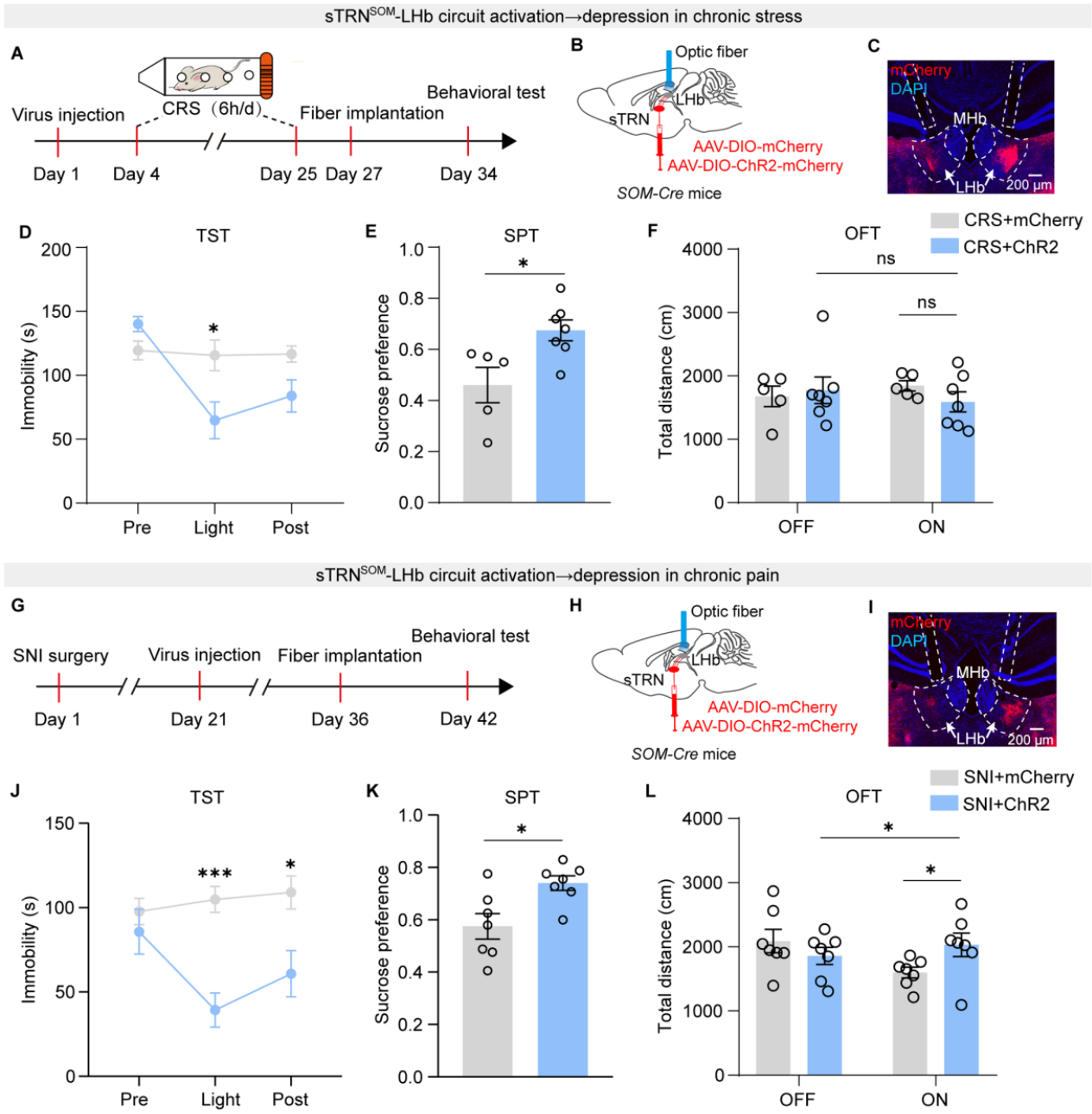

Figure 4. Activation of the sTRN^{SOM}-LHb circuit alleviates depressive-like behaviors induced by chronic stress and by chronic pain.

(A and G) Schematic of experimental design.

(B and C) Illustration (B) and representative image (C) of viral delivery and bilateral optic fibers implantation. Scale bar, 200 μm.

(D-F) Behavioral effects of optogenetic activation of LHb-projecting sTRN^{SOM} neural afferents on depressive-like behaviors assessed by TST (D) and SPT (E), and locomotion activity assessed by OFT (F) in CRS-treated *SOM-Cre* mice. (n=5-7 mice/group)

585 (H and I) Illustration (H) and representative image (I) of viral delivery and bilateral
586 optic fibers implantation. Scale bar, 200 μm.
587 (J-L) Behavioral effects of optogenetic activation of LHb-projecting $sTRN^{SOM}$ neural
588 afferents on depressive-like behaviors assessed by TST (J) and SPT (K), and
589 locomotion activity assessed by OFT (L) in SNI-treated *SOM-Cre* mice. (n=7
590 mice/group)
591 Data are presented as mean ± SEM. "ns", no significance; *$p < 0.05$, ***$p < 0.001$.
592 Two-way repeated measures ANOVA with Bonferroni *post hoc* analysis for (D), (F),
593 (J) and (L); Unpaired two-sided t test for (E) and (K).

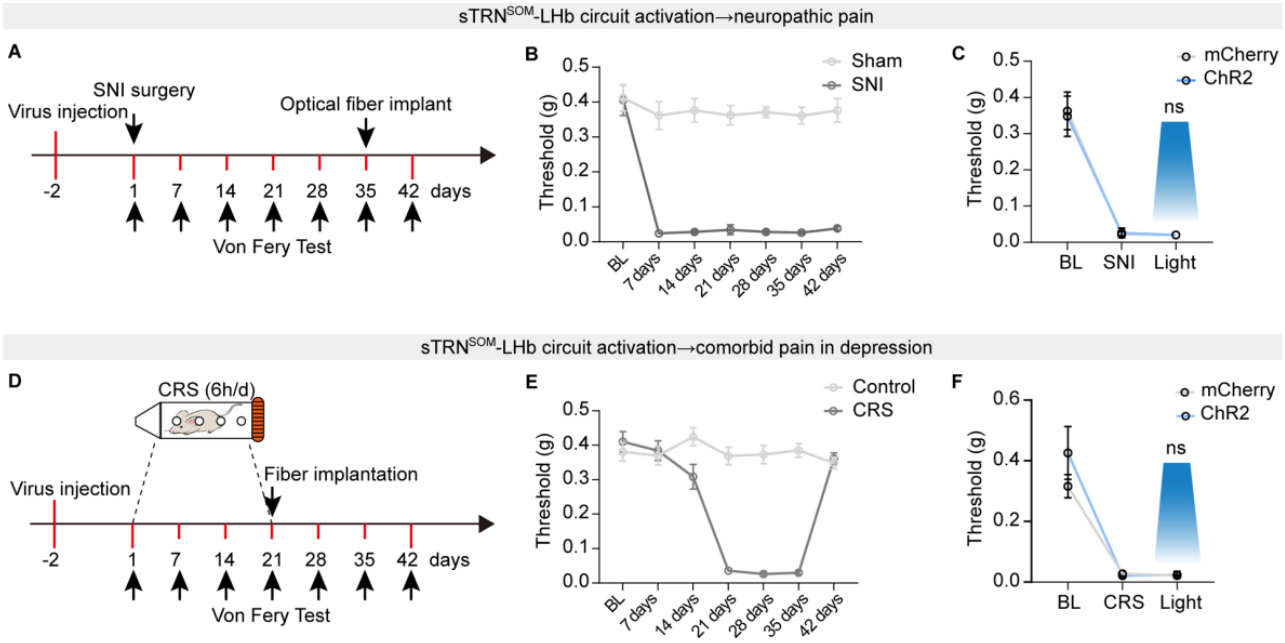

Figure 5. Activation of the sTRN^{SOM}-LHb circuit does not affect pain induced by nerve injury and by depression.

(A and D) Schematic of experimental design.

(B) Mechanical hypersensitivity in SNI-treated *C57* mice. (n=7-10 mice/group)

(C) Behavioral effects of optogenetic activation of LHb-projecting sTRN^{SOM} neural afferents on pain-like behavior assessed by von Frey test in SNI-treated *SOM-Cre* mice. (n=5-7 mice/group)

(E) Comorbid pain-like behavior in CRS-treated *C57* mice. (n=5-8 mice/group)

(F) Behavioral effects of optogenetic activation of LHb-projecting sTRN^{SOM} neural afferents on pain-like behaviors assessed by von Frey test in CRS-treated *SOM-Cre* mice. (n=5-7 mice/group)

Data are presented as mean ± SEM. “ns”, no significance; *$p < 0.05$, ***$p < 0.001$. Two-way repeated measures ANOVA with Bonferroni *post hoc* analysis.

Methods

Animals

Adult (8-10 weeks) C57BL/6J, *SOM-Cre*, *PV-Cre*, *CaMKIIα-Cre* and *Rosa*26-tdTomato *(Ai14)* male mice were used in this study. *C57BL/6J* mice were purchased from Beijing Vital River Laboratory Animal Technology, *Ai14*, *SOM-Cre*, *PV-Cre* and *CaMKIIα-Cre* mice were initially acquired from the Jackson Laboratory. Animals were maintained in a stable room temperature (23 ± 1 °C) with a 12-hour light/dark cycle (lights on from 7:00 to 19:00). They were housed five per cage in a colony with ad libitum water and food. All animal experiment procedures were approved by the animal care and use committee of the University of Science and Technology of China.

Animal models

Chronic restraint stress model (CRS)

Mice were placed in restraint tubes made of 50 ml centrifuge tubes for 6 hours (from 9:00 to 15:00) per day for consecutive 21 days. The centrifugal tube is pre-stamped with air holes scattered throughout the tube to allow the mouse to breathe, and there is a small hole in the center of the lid through which the mouse's tail is exposed to air (see Figure S3A). During the restraint period, control mice were allowed to freely move around the cage, but fasting for water and food. At the end of 21 days, the mice were allowed to take 1 day off to exclude the effects of acute stress.

Spared nerve injury model (SNI)

Spared nerve was injured following the protocol previously described (Bourquin et al., 2006). In brief, the mice were anesthetized with 3% isoflurane. Incision was made in the middle of the left thigh using the femur as a marker. The skin and muscle were incised to explore the sciatic nerve comprising the sural, common peroneal, and tibial nerves. The tibial and common peroneal nerves were ligated with nonabsorbent 4-0 chromic gut and transected (1-2 mm slices), while the sural nerve was carefully preserved. The skin was sutured with 6-0 silk and disinfected by iodophor. For the sham group, the procedure was the same as for the experimental group except ligation

636 and transection of the nerves.

637 **Stereotaxic surgeries**

638 Before surgery, the mice were fixed in a stereotactic frame (RWD, Shenzhen, China)
639 under anesthesia with 3% pentobarbital sodium (30 mg/kg) intraperitoneally (i.p.),
640 and body temperature was maintained with a heating pad. Erythromycin eye ointment
641 was applied to maintain eye lubrication. The skull surface was exposed with a midline
642 scalp incision, and the injection site was defined using stereotactic coordinates (see
643 below). Adental drill (RWD, DC 30V) was used for craniotomy (~0.5 mm hole) to
644 enable virus injection. Injections of 150-200 nl virus (depending on the expression
645 strength and viral titer) were carried out through the glass pipettes (tip diameter of
646 10-30 μm) connected to an infusion pump (KD Scientific) at a rate of 50 nl/min. After
647 the injection is completed, the glass pipettes were left for 10 min before withdrawal to
648 allow virus diffusion. The mice were allowed to recover from anesthesia on a heating
649 blanket before returning to the home cage. The coordinates were defined as
650 dorso-ventral (DV) from the brain surface, anterior--posterior (AP) from bregma and
651 medio-lateral (ML) from the midline (in mm).

652 **Virus injection and optical fibers implantation**

653 To manipulate the activity of sTRN and LHb neurons, adenoassociated viruses (AAVs)
654 were injected unilaterally or bilaterally into the sTRN (AP: -1.5 mm; ML: ±2.35 mm;
655 DV: -3.3 mm) and LHb (AP: -1.9 mm; ML: ± 0.45 mm; DV: -2.65 mm), and
656 behavioral tests were performed 2-3 weeks later.

657 **Viral injection**

658 For pharmacogenetic inhibition or activation of LHb neurons, mice were bilaterally
659 microinjected with 150 nl of rAAV2/9-EF1α-DIO-hM4Di-mCherry-WPREs (titer:
660 5.18E+12 vg/ml, BrainVTA, PT-0043) or
661 rAAV2/9-Ef1α-DIO-hM3Dq-mCherry-WPREs (titer: 5.27E+12 vg/ml, BrainVTA,
662 PT-0042) , and rAAV2/9-EF1α-DIO-mCherry-WPRE-pA (titer: 5.14E+12 vg/ml,
663 BrainVTA, PT-0013) as a control into the LHb. For pharmacogenetic inhibition of

664 LHb glutamatergic neurons, mice were bilaterally microinjected with 150 nl of
665 rAAV2/9-CaMKIIa-hM4Di-mCherry-WPREs (titer: 5.91E+12 vg/ml, BrainVTA,
666 PT-0050), and rAAV2/9-CaMKIIa-mCherry-WPRE-pA (titer: 5.14E+12 vg/ml,
667 BrainVTA, PT-0108) as a control into the LHb. For chemogenetic manipulation of
668 LHb activity, mice were injected with clozapine N-oxide (CNO, i.p., 2 mg/kg,
669 APExBIO Technology LLC).

670 For optogenetic stimulation, mice were bilaterally microinjected with 150 nl of
671 rAAV2/9-EF1α-DIO-hChR2(H134R)-mCherry-WPRE-pA (titer: 4.50E+12 vg/ml,
672 BrainVTA, PT-0002) or rAAV2/9-EF1α-DIO-eNpHR3.0-EYFP-WPRE-pA (titer:
673 5.36E+12 vg/mL, BrainVTA, PT-0006) into the sTRN.

674 For monosynaptic anterograde tracing, we microinjected 250 nl of
675 rAAV2/1-hSyn-Cre-WPRE-pA (titer: 1.00E+12 vg/mL, BrainVTA, PT-0136) into the
676 unilateral sTRN of C57BL/6J mice. The rAAV2/9-EF1α-DIO-mCherry-WPRE-pA
677 (titer: 5.14E+12 vg/mL, BrainVTA, PT-0013) was subsequently delivered into the
678 LHb. For monosynaptic retrograde tracing, we microinjected 200 nl of
679 rAAV2/2-retro-hSyn-Cre-WPRE-pA (titer: 5.22E+12 vg/ml, BrainVTA, PT-0136)
680 into the unilateral LHb of C57BL/6J mice. The
681 rAAV2/9-EF1α-DIO-mCherry-WPRE-pA (titer: 5.14E+12 vg/ml, BrainVTA,
682 PT-0013) was subsequently delivered into the sTRN. For sTRN upstream brain region
683 dissection, 150 nl of rAAV2/2-retro-hSyn-Cre-WPRE-pA (titer: 5.77E+12 vg/ml,
684 BrainVTA, PT-0136) was injected into sTRN of *Ai14* mice.

685 **Optical fibers implantation**

686 For optogenetic manipulation in awake behaving mice, chronically optical fiber
687 (diameter, 200 μm; N.A., 0.37; length, 4 mm; Inper) were implanted 200 μm above
688 the virus injection site in the bilateral LHb (AP: -1.9 mm; ML: ± 1.1mm; DV: -2.45
689 mm at an angle of 15°). The fibers were attached to the skull with dental cement and
690 connected to a laser generator using an optical fiber sleeve. The delivery of a 5-min
691 pulse of blue light (473 nm, 1-3 mW, 15 ms pulses, 20 Hz) or yellow light (594 nm,
692 5-8 mW, 15 ms pulses, 20 Hz) was controlled by a class laser product

693 (QAXK-LASER, ThinkerTech). The same stimulus protocol was applied in the
694 control group. Following surgery, the mice were allowed to recover at least 1 week
695 before performing the behavioral experiments. We checked the location of fibers after
696 all experiments and discarded the data obtained from mice in which the fibers were
697 outside the desired brain region.

698 **Fiber photometry recording**

699 The three-color single-channel fiber photometry system (ThinkerTech) was used for
700 recording Ca^{2+} signals from LHb neurons or LHb-projecting TRN afferents. The 150
701 nl of rAAV2/9-hSyn-GCaMP6m-WPRE-pA (titer: 5.51E+12 vg/ml, BrainVTA,
702 PT-0148) virus was injected into the sTRN (AP: -1.5 mm; ML: +2.35 mm; DV: -3.25
703 mm) of C57BL/6J mice or into the LHb (AP: -1.9 mm; ML: +0.45 mm; DV: -2.55
704 mm) of *CaMKIIα-Cre* mice, an optical fiber (diameter: 200 μm; N.A., 0.37; length, 4
705 mm; Inper) was subsequently implanted into the sTRN or LHb. The optical fiber was
706 affixed with a skull-penetrating screw and with dental acrylic. To enable recovery and
707 AAV expression, mice were housed individually for at least 10 days following virus
708 injection. After three weeks, the fiber photometry data were recorded continuously
709 during the air puff, pinch and physical restraint tests. The normalized Delta F/F values
710 and traces were visualized using custom MATLAB (MathWorks) scripts that were
711 produced by ThinkerTech. In addition, we excluded the mice that had no GCaMP6m
712 signals in response to air puff stimuli on their paws before performing tests, which
713 may be due to the failure of viral expression and missed targets, including the
714 injection of viruses, placement of optical fiber or optical fiber tip clogging.

715 **Depression-related behaviors test**

716 For all behavioral tests, dim light (20 lux) and a quiet environment were used in the
717 room to minimize the anxiety of the animals. The behavioral experiments described
718 herein were performed by experimenters who were blind to the treatments.

719 **Open field test (OFT)**

720 Motor activity was tested in open field test box (40×40×40cm). Individual mice were

introduced into the center of the box in a room with dim light and were allowed to freely explore their surroundings during 6 min test session with a video-tracking system. The duration that animal spent in the central area and total distance traveled to the central area in the last 5 min were analyzed by SMART V3.0 software (Panlab). To remove olfactory interference, we cleaned the box with 75% ethanol after each test. To examine the effect of optogenetic experiment on mouse locomotion, laser was delivered from the 6th to 11th min in 16 min-period OFT test.

Forced swim test (FST)

Mice were individually placed into a transparent plexiglass cylinder (diameter 12 cm, height 30 cm), containing a height 20 cm of water at 24 ± 2℃. In the test, the time of swimming and immobility was measured during a 6 min period. The processes were videotaped from the side. Immobility was assigned when no additional activity was observed other than that required to keep the mice head above the water. The time that mice spent in immobility in the last 5 min was quantified offline manually by an observer blinded to animal treatment. Animals were never allowed to drown during the test. Mice with nerve injury were exempted from the FST because of the undermined swimming skill.

Tail suspension test (TST)

Mice were suspended by the tip of tail using adhesive tape. One end of the tape was attached to a horizontal table that surface above 30 cm from the floor. During the 6 min process, the behavior was videotaped from the side. The immobile time during the last 5 min was manually recorded by an observer blinded to animal treatment. Mice were considered immobile when they were completely motionless or passive swaying. For optogenetic manipulations, mice were first hung by the tail for 2 min, followed by a 3 min off/ 3 min on/ 3 min off light epoch.

Sucrose preference test (SPT)

The animals were housed in a single cage and given two bottles of distilled water for 48 h training, then two bottles of 1% sucrose water for 48 h training. After 24h of water deprivation, the final test was performed for 2 h, giving one bottle of water and

750 one bottle of 1% sucrose water. The positions of the two water bottles were
751 exchanged halfway through the period of 1 h. The sugar-water preference index was
752 calculated as the ratio of 1% sucrose water to the total water (water and sucrose water)
753 consumed. For the optogenetic experiment, mice were subjected to a 30-minute light
754 period and sugar-water preference index was measured.

755 **Mechanical allodynia assay**

756 Prior to behavioral testing, all animals were habituated to plexiglass chambers
757 (6.5×6.5×6 cm) positioned on a wire mesh grid for at least two days. Once the mice
758 were calm, the plantar area of hind paws was stimulated with a series of Von Frey
759 filaments with different strength (g) to measure the mechanical withdrawal threshold.
760 The stimulus producing a 50% likelihood of a withdrawal response was determined
761 and taken as the paw withdrawal threshold (PWT) using the Up-Down method
762 (Chaplan et al., 1994).

763 **Immunofluorescence and imaging**

764 Mice were deeply anesthetized with 3% isoflurane and then intracardially perfused
765 with 20 ml 0.01M phosphate-buffered saline (PBS) (4℃) and 20 ml 4%
766 paraformaldehyde (PFA) in PBS (4℃). After post-fixation overnight, the mouse brain
767 was cryoprotected with 30% sucrose for two days. The brain was embedded in OCT
768 (SAKURA, 4583) and sectioned coronally (30 μm thick) with a freezing microtome
769 (Leica CM1950). For immunofluorescent staining, the sections were blocked with 3%
770 BSA in PBS with 0.3% Triton X-100 for 1h at room temperature and subsequently
771 incubated with primary antibodies (rabbit anti-VGLUT2, 1:500, Sigma; rabbit
772 anti-SOM, 1:500, Novus; rabbit anti-c-Fos, 1:500, Synaptic Systems) at 4˚C overnight.
773 After washing with PBS, the sections were subsequently coupled with the
774 corresponding fluorophore-conjugated secondary antibodies (1:500, Jackson) for 1.5 h
775 at room temperature. Finally, after washing 3 times for 7 min in PBS, sections stained
776 with DAPI, and the slides were sealed with anti-fluorescence quenching sealing
777 tablets. Images were captured with Olympus confocal microscopes (FV3000,

Olympus) and analyzed with ImageJ software.

Brain slice electrophysiology

Brain slice preparation

For slices preparation, mice were anesthetized with isoflurane followed by pentobarbital (30 mg/kg, i.p.) and intracardially perfused with ~20 ml oxygenated ice-cold modified N-methyl-D-glucamine and artificial cerebrospinal fluid (NMDG ACSF) that contained (in mM) 93 NMDG, 2.5 KCl, 1.2 NaH_2PO_4, 30 $NaHCO_3$, 20 N-2-hydroxyethylpiperazine-N-2-ethanesulfonic acid (HEPES), 25 glucose, 5 Na-ascorbate, 3 Na-pyruvate, 0.5 $CaCl_2$, 10 $MgSO_4$, 3 glutathione (GSH) and 2 thiourea (pH: 7.3-7.4, osmolarity: 300-310 mOsm). Coronal slices (300 μm) containing the sTRN or LHb were sectioned in chilled (2-4℃) NMDG ACSF at 0.18 mm/s velocity on a vibrating microtome (VT1200s, Leica). The brain slices were initially incubated in NMDG ACSF (saturated with 95% O_2/5% CO_2 to provide stable potential of hydrogen and continuous oxygenation) for 10 min at 33 °C, followed by (HEPES) ACSF that contained (in mM) 92 NaCl, 2.5 KCl, 1.2 NaH_2PO_4, 30 $NaHCO_3$, 20 HEPES, 25 glucose, 2 thiourea, 5 Na-ascorbate, 3 Na-pyruvate, 2 $CaCl_2$, 2 $MgSO_4$ and 3 GSH (pH 7.3-7.4, osmolarity 300-310 mOsm) for at least 1 h at 25 °C. The brain slices were transferred to a slice chamber for electrophysiological recording and were continuously submerged and superfused with standard ACSF that contained (in mM) 129 NaCl, 2.4 $CaCl_2$, 3 KCl, 1.3 $MgSO_4$, 20 $NaHCO_3$, 1.2 KH_2PO_4 and 10 glucose (pH 7.3-7.4, osmolarity 300–310 mOsm) at 5 ml/min at room temperature. During recording and analysis, the recorders were blind to group identity.

Electrophysiological verification of pharmacogenetics and optogenetics

Whole-cell patch-clamp recordings were obtained from visually identified sTRN or LHb cells. Neurons in the slice were visualized using a ×40 water-immersion objective on an upright microscope (BX51WI, Olympus) equipped with infrared-differential interference contrast (IR-DIC) and an infrared camera connected to the video monitor. Patch pipettes (6-8 MΩ) were pulled from a horizontal puller (P1000, Sutter Instruments) and filled with the internal solution that contained (in

807 mM): 130 K-gluconate, 5 KCl, 4 Na_2ATP, 0.5 NaGTP, 20 HEPES, 0.5 EGTA, (PH
808 7.28, 290-300 mOsm). Whole-cell patch-clamp recordings were acquired via a
809 Multiclamp 700B patch-clamp amplifier (Molecular Devices) and Digidata 1550B
810 (Molecular Devices), digitized at 5 kHz, and filtered at 2 kHz. Data were analyzed
811 with pClamp 10.0 software. Cells were excluded when series resistance changed more
812 than 20% during the recording.

813 To confirm the efficacy of ChR2-mediated activation, fluorescently labeled neurons
814 that expressed ChR2 in *SOM-Cre* mice 3 weeks after virus injection were visualized
815 and stimulated with a 473 nm laser (QAXK-LASER, China) using 20 Hz stimulation
816 protocols with a pulse width of 15 ms. After a stable membrane potential was
817 acquired, 473-nm laser illumination induced reliable spikes in TRN neurons. Similarly,
818 the functional expression of eNpHR3.0 was assessed by applying yellow (594 nm)
819 laser light stimulation. To confirm the efficacy of hM4Di-mediated inhibition and
820 hM4Dq-mediated excitation, CNO (10 μM; APExBIO Technology LLC) was
821 bath-applied.

822 To examine firing rate of LHb neurons, 500 ms pulses with 10 pA command
823 current steps were injected from -60 to +150 pA, and the numbers of spikes were
824 quantified for each step.

825 To examine functional inhibitory projections from the sTRN to the LHb, membrane
826 potentials of LHb neurons were held at 0 mV to record light-evoked IPSCs. For
827 evaluating synaptic identities, GABA-mediated IPSCs were blocked by the bath
828 application of bicuculline (10 μM, Sigma). To test direct synaptic connections, both
829 TTX (1 μM, Sigma) and 4-AP (500 μM, Sigma) were used to restore monosynaptic
830 current.

831 **Quantification and statistical analysis**

832 All experiments and data analyses were conducted blindly, including the
833 immunohistochemistry, electrophysiology and behavioral analyses. Data were
834 analyzed with GraphPad Prism v.8.0.1, Olympus FV10-ASW 4.0a Viewer, Microsoft
835 office 2021, and MATLAB R2016a software. Behavioral data were analyzed by

one-way or two-way analysis of variance (ANOVA) followed by Bonferroni's test for multiple comparisons, and the unpaired Student's t-test for two group comparisons. Imaging of calcium activity data were analyzed by paired Student's t-test. For immunofluorescence analysis, data were analyzed using unpaired Student's t-test. Statistical significances were represented as *$p < 0.05$, **$p < 0.01$, ***$p < 0.001$, ****$p < 0.0001$. All data were expressed as mean ± standard error of means (S.E.M.) except for data in Figure 1E and 1G shown as box and whisker plots.

Acknowledgments: This study was supported by the National Natural Science Foundation of China (grants 32271048 and 32070999 to Yan Z, U20A20357 to X. F. L, 31972905 and 32271190 to Ying Z.) and Anhui Provincial Natural Science Foundation (grant 2008085J16 to Yan Z.).

Author contributions: X. X., R. C. and X. Y. W. designed the studies and conducted most of the experiments and data analysis. X. X. and R. C. wrote the first draft. W. B. J. and P. F. X generated some behavioral data. X. Q. L. managed the mouse colonies used in this study. Ying Z., X. F. L. and Yan Z. were involved in the overall design of the project and editing of the final manuscript.

Declaration of interests

The authors declare no competing interests.

All data necessary to understand and assess the conclusions of this study are available in the main text or the supplementary materials. There are no restrictions on data availability in the manuscript.